Thermal Characterization of Diamond Films through Modulated Photothermal Radiometry

Thomas Guillemet,*,†,‡,§ Andrzej Kusiak,⊥ Lisha Fan,§ Jean-Marc Heintz,† Namas Chandra,§ Yunshen Zhou,§ Jean-François Silvain,† Yongfeng Lu,‡ and Jean-Luc Battaglia⊥

†Institut de Chimie de la Matière Condensée de Bordeaux, CNRS, Université de Bordeaux, 33608 Pessac, France
⊥Department TREFLE, Institut de Mécanique et Ingénierie, 33400 Talence, France
‡Department of Mechanical and Materials Engineering, University of Nebraska−Lincoln, Lincoln, Nebraska 68588-0511, United States
§Department of Electrical Engineering, University of Nebraska−Lincoln, Lincoln, Nebraska 68588-0511, United States

Ⓢ Supporting Information

ABSTRACT: Diamond (Dia) films are promising heat-dissipative materials for electronic packages because they combine high thermal conductivity with high electrical resistivity. However, precise knowledge of the thermal properties of the diamond films is crucial to their potential application as passive thermal management substrates in electronics. In this study, modulated photothermal radiometry in a front-face configuration was employed to thermally characterize polycrystalline diamond films deposited onto silicon (Si) substrates through laser-assisted combustion synthesis. The intrinsic thermal conductivity of diamond films and the thermal boundary resistance at the interface between the diamond film and the Si substrate were investigated. The results enlighten the correlation between the deposition process, film purity, film transverse thermal conductivity, and interface thermal resistance.

Pt transducer (30 nm)
Diamond film (4 μm)
Si (wafer)
5 μm

KEYWORDS: diamond films, laser-assisted combustion synthesis, interface, heat conduction
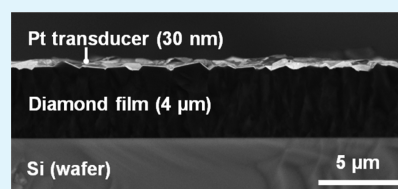
1. INTRODUCTION

Diamond (Dia) films are highly attractive materials for passive heat-dissipative substrate applications in electronic packages. Diamond combines, in a very particular way, high electrical resistivity ($\rho = 10^{11}-10^{13}$ Ω·cm)[1] with excellent thermal conductivity ($\lambda = 800-2000$ W·m^{-1}·K^{-1}),[1] ideally providing efficient paths for heat flux without compromising the electrical insulation of active components. Moreover, diamond exhibits a low coefficient of thermal expansion [CTE; $\alpha = (1-2) \times 10^{-6}$ °C^{-1}] that is close to that of typical semiconductor materials, such as silicon (Si) or gallium arsenide, thus allowing thermomechanical stresses, due to CTE mismatch between a diamond heat spreader and an active chip, to mitigate.[2]

Various chemical vapor deposition (CVD) techniques for growing diamond films on bulk substrates have emerged since the early 1980s, including hot-filament deposition, microwave-plasma-assisted deposition, plasma jet deposition, and combustion flame deposition. These techniques all combine three main components: a substrate, a source of carbon precursors, and a source of activation energy. The diamond growth process relies on the ability to set up a dynamic nonequilibrium system in which only sp^3 carbon bonding can survive. This is achieved by the presence of hydrocarbon radicals that provide the carbon source for diamond deposition and, more importantly, by large quantities of atomic hydrogen in the deposition gas. Hydrogen is indeed the key element in these CVD processes because it stabilizes the growing diamond surface while suppressing the growth of graphitic carbon. By the creation of a plasma system where atomic hydrogen predominates, any graphitic bonding is etched away, leaving only high-quality diamond.[2]

CVD synthesis methods widen the scope of potential diamond film applications in electronics by decreasing the capital cost of diamond synthesis, increasing its scalability and manufacturability, and providing synthetic diamond materials with high phase purity and high thermal performance. Therefore, CVD synthesis has opened promising possibilities for diamond film applications as heat-dissipative substrate materials. Moreover, the constant increase in operating speed (higher frequency) and integration level (higher power) and decrease in feature size (higher packing density) of integrated circuits lead to continuous increases in power and heat flux densities in electronic packages. This drives a rising demand for materials with enhanced heat dissipation performance able to ensure the reliability and lifetime of high-power devices. A free-standing, thick CVD diamond substrate can be attached to a semiconductor-active device through soldering, or a diamond film can be directly coated onto it. In past years, CVD diamond films have proven efficient as passive heat-dissipative materials for optoelectronic,[3] microelectronic,[4] and high-power electronic packaging applications.[5,6]

The design of an efficient electronic package involving diamond as the heat-dissipative material requires accurate

knowledge of its thermal properties. Numerous techniques have been employed to determine the thermal conductivity of CVD diamond films, among them joule-heating thermometry,[7] a photoacoustic method,[8] simple thermocouple routes,[9,10] photothermal microscopy,[11] and holographic interferometry.[12] Polycrystalline CVD diamond films typically exhibit thermal conductivity ranging between 300 and 700 W·m^{-1}·K^{-1},[7−10] which is higher than most electronic packaging materials but considerably lower than the thermal conductivity values recorded for natural diamond. The thermal conductivity gap existing between CVD diamond films and natural diamond is known to originate from the particular microstructure and composition exhibited by CVD diamond films.[13,14] Indeed, phonons that carry heat into diamond may be scattered in various ways. Point imperfections, such as vacancies, impurities, interstitials, and isotopes, line imperfections, such as dislocations, and surface imperfections, such as grain or twin boundaries, act as many phonon scatterers, decreasing the phonon mean-free path and thus affecting the heat conduction process through diamond.[15] The relatively lower thermal conductivity exhibited by synthetic CVD diamond films is also revealed by their typical black color, indicating a high amount of nondiamond carbon content.[11] Nevertheless, polycrystalline CVD diamond films exhibiting thermal conductivity as high as 1100 W·m^{-1}·K^{-1} have been recorded.[7,12,15,16]

Most of the thermal conductivity data gathered about diamond films concern deposits obtained either through microwave-plasma-assisted or hot-filament techniques, and diamond films grown through combustion flame synthesis suffer from a lack of thermal conductivity characterization in the literature. Unlike combustion CVD, which is an open-air process, hot-filament- and microwave-assisted CVD routes involve vacuum environments that are highly desirable when seeking to grow electronic-quality materials. Diamond films grown through combustion CVD usually suffer from moderate quality because of their high nondiamond carbon content. Nevertheless, combustion CVD provides some positive features, such as low capital costs and high growth rates, which are key assets to the applicability of diamond films. Moreover, laser-assisted combustion CVD may allow, at certain laser excitation wavelengths, selection from among the various competing chemical processes for diamond growth in the flame environment, possibly leading to the deposition of high-phase-purity diamond films, which would be strongly desirable for electronic applications.

While thermal conductivity is extensively examined when characterizing diamond films under a thermal prospective, very few studies have focused on estimating the thermal boundary resistance (TBR) existing at the diamond film/substrate interface, despite the critical role it plays in the heat conduction process through such layered assemblies.[17,18] Goodson et al.[19] pointed out the shortage of existing data on thermal resistance at the boundaries of CVD diamond films. They developed a pulsed laser-heating measurement technique to investigate the heat conduction process normal to metallized diamond films grown on Si substrates through microwave-plasma-assisted deposition at 830 °C and determined the thermal resistance at the Dia/Si interface. Goodson et al. reported TBR values of 1.7 × 10^{-8} K·m^2·W^{-1} for a 0.2-μm-thick diamond film and up to 3.5 × 10^{-8} K·m^2·W^{-1} for a 2.6-μm-thick diamond film. Finally, they established that the details of the diamond deposition process had a great influence on transverse heat conduction

through Dia/Si assemblies, especially in terms of the nucleation density and grain size. Verhoeven et al.[20] measured TBRs of 1.1 × 10^{-8} K·m^2·W^{-1} for diamond films deposited at low temperature (~500 °C) on Si using microwave-plasma-assisted CVD and 2.0 × 10^{-7} K·m^2·W^{-1} for diamond films deposited through electron-cyclotron-resonance-enhanced microwave-plasma-assisted CVD. In the same manner, Stoner et al.[21] evaluated the thermal resistance at the interface between the diamond and some metals at room temperature. The measured TBRs were reported to be 3.33 × 10^{-8} K·m^2·W^{-1} at the Dia/Pb interface, 4.0 × 10^{-8} K·m^2·W^{-1} at the Dia/Au interface, 4.6 × 10^{-8} K·m^2·W^{-1} at the Dia/Al interface, and 1.0 × 10^{-7} K·m^2·W^{-1} at the Dia/Ti interface.

In this study, a multienergy diamond deposition process was achieved by associating a wavelength-tunable CO$_2$ laser to a combustion flame, thus combining sources of electromagnetic and thermal energy. The laser wavelength was tuned to 10.532 μm in order match a vibrational mode of carbon precursor molecules. Laser-resonant excitation has been demonstrated to promote growth rates and enhance the diamond phase purity relative to traditional combustion flame deposition.[22,23] This phenomenon originates from the laser-induced resonant excitation of a vibrational mode of carbon precursor molecules that triggers an increase in diamond growth active species into the flame chemical environment (hydrocarbon radicals, atomic hydrogen). Modulated photothermal radiometry (MPTR)[24,25] in a front-face configuration was used to determine the transverse thermal conductivity and the TBR of polycrystalline diamond grown onto Si substrates. Finally, these thermal properties were correlated with their processing conditions, chemical composition, and microstructure.

2. MATERIALS AND METHODS

2.1. Diamond Film Deposition. Diamond films were grown on Si substrates through open-air, laser-assisted combustion synthesis. The experimental setup is depicted in Figure 1 and consists of a
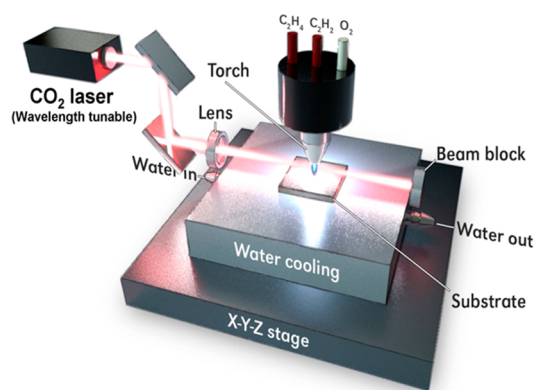

Figure 1. Experimental setup for diamond film deposition through laser-assisted combustion synthesis.

wavelength-tunable CO$_2$ laser (XL1000, PRC Laser Corp.) associated with a combustion torch with a diameter of 1.5 mm. A gas mixture containing acetylene (C$_2$H$_2$, 99.999%), ethylene (C$_2$H$_4$, 99.6%), and oxygen (O$_2$, 99.996%) was used as a gas precursor for diamond growth with a volume ratio of 1:1:2, respectively. The laser beam was guided through the combustion flame using a ZnSe convex lens with a focal distance of 25.6 cm. The distance between the lens and the nozzle was 30 cm. The distance between the flame inner cone and the top of the substrate was maintained around 0.8 mm. The laser was operated in a continuous-wave mode. Its output power was 800 W, and its
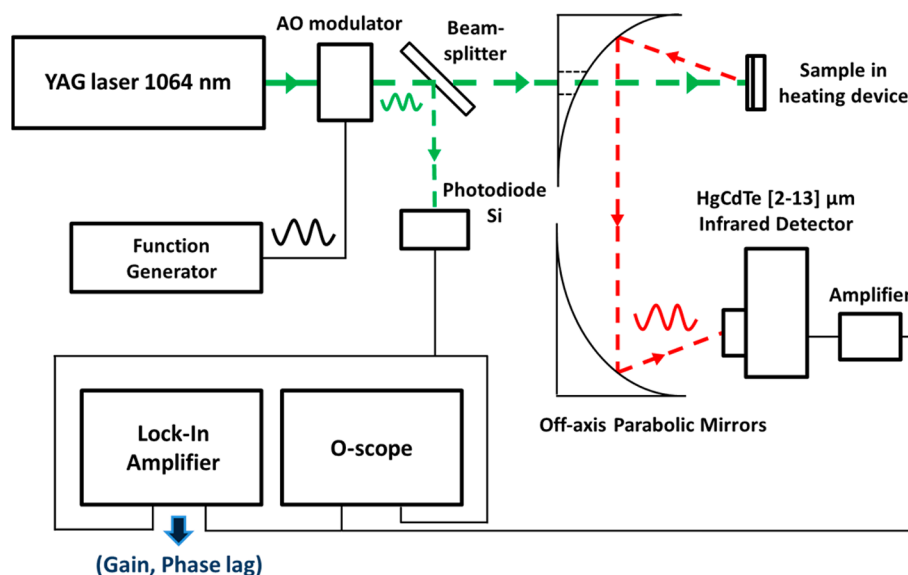
2096

dx.doi.org/10.1021/am405188r | ACS Appl. Mater. Interfaces 2014, 6, 2095−2102

Figure 2. Experimental setup for thermal characterization of diamond films through MPTR.

wavelength was set to 10.532 μm in order to match the wagging vibrational mode of C_2H_4 ethylene molecules, thus achieving laser-induced resonant excitation of the ethylene molecules. The substrate temperature was monitored using an IR pyrometer (OS3752, Omega Engineering, Inc.) and regulated using a water-cooling stage. The stage was attached to an X−Y−Z translation system to position the substrate toward the torch. The substrate temperature was maintained around 780 °C during diamond deposition. More details about the laser-assisted combustion synthesis route used in this study are available in previous publications.[22,23]

Diamond films were deposited on commercial Si(100) wafers. Si substrates were chosen because they are the most important active chip material used by the contemporary semiconductor industry. The dimensions of the Si substrates were $10 \times 10 \times 0.6$ mm^3. Diamond films were grown on Si substrates as circular spots of about 1 cm diameter. The deposition times were 10, 20, 40, and 50 min, leading to diamond films with thicknesses of 5, 10, 12.5, and 15 μm, respectively. The substrates were ultrasonically cleaned for 20 min in acetone prior to diamond deposition. Si substrates were laser-roughened using a pulsed femtosecond laser source prior to deposition in order to enhance the nucleation of diamond crystals on the Si(100) surfaces. Details about the laser-roughening process and about the laser-induced surface structures are available in a different publication.[26] The microstructure of the diamond films deposited were investigated using scanning electron microscopy (SEM; Vega Tescan). Film thicknesses and roughnesses were measured using a stylus profiler (XP-2, Ambios Technology). Elemental analyses were carried out on both sides of a delaminated Si/Dia interface through Auger electron spectroscopy (AES; Thermo Microlab 310F). Information relative to the phase purity of the diamond films deposited was obtained through Raman spectroscopy analyses. More details about the Raman system employed are available in previous studies.[20]

2.2. Thermal Characterization Technique. The MPTR experimental setup is schematically depicted in Figure 2. The heat source was a continuous YAG laser of 1064 nm wavelength and 5 W maximum power. The laser beam was modulated in intensity by an acoustooptic modulator in the range $f = 0.7−21$ kHz and was brought to the sample surface by a set of mirrors. The laser beam had a Gaussian profile of power distribution on the spot of 3 mm diameter at $1/e^2$. The thermal response was measured through an IR HgCdTe detector. The wavelength detection limits of this IR detector ranged between 2 and 13 μm, with a maximum detection wavelength of 11 μm. Parabolic mirrors were used to collect the IR radiation emitted and focus it on the IR detector. The area in the scope of the IR detector corresponded to a circle of 0.5 mm diameter of the excited

zone of the sample. Finally, a lock-in amplifier was used to measure the amplitude of the thermal response and the phase lag between the reference signal from a photodiode and the signal from the IR detector. More details about the MPTR experimental setup are available in previous studies.[24,25] A 100-nm-thick platinum (Pt) layer was deposited on the top surface of the diamond films through physical vapor deposition to act as an optical and thermal transducer and thus increase the signal-to-noise ratio during MPTR.

The heat-transfer model in the sample was a two-dimensional (2D) model based on the classical linear heat diffusion equation in the three-layer system composed of the Pt film, diamond layer, and Si substrate. The model was solved analytically using Laplace transforms for the time variable and Hankel transforms for the radial direction. Therefore, the average measured temperature on the front face of the sample was obtained according to the heat flux in the frequency domain. The transverse thermal conductivity of the diamond film (k_{Dia}), as well as the TBR at the interfaces between the Pt transducer and the diamond film ($R^i_{Pt/Dia}$) and between the diamond film and the Si substrate ($R^i_{Dia/Si}$), was obtained by minimizing the gap between the measured phase and amplitude and those calculated through the Levenberg−Marquardt algorithm.[27] The radial thermal conductivity, although accessible through the 2D model, could not be precisely estimated, and the measured thermal conductivity is approximated by the transverse thermal conductivity of the deposit. This does not prevent a precise estimation of the TBRs in the Pt/Dia/Si-layered samples. More details about the 2D heat-transfer model adopted in this study and the mathematical procedure to retrieve the thermal parameters are provided in the Supporting Information (SI).

3. RESULTS AND DISCUSSION

3.1. Diamond Film Microstructure and Phase Purity. SEM micrographs of diamond films deposited on Si substrates through laser-assisted combustion synthesis are shown in Figure 3. They show that the laser-assisted deposition process enabled the deposition of thick diamond films onto the Si substrates in an open-air environment. The resulting diamond films exhibited a polycrystalline microstructure consisting of randomly oriented diamond crystals, as shown on the top-surface SEM micrograph in Figure 3a. The films exhibited the typical black color of CVD diamond films, revealing the nondiamond carbon content embedded in the films. The films were observed to be dense, without voids or cavities. The Dia/Si interface also exhibited good integrity, without obvious voids
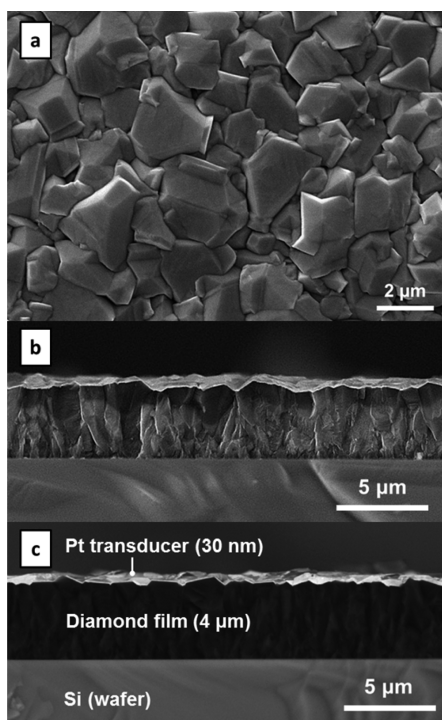
Figure 3. Micrographs of a diamond film deposited onto a Si substrate through laser-assisted combustion synthesis: (a) top-surface SE micrograph; (b) cross-sectional SE micrograph; (c) cross-sectional BSE micrograph.

or holes in the film or around the substrate interface, as shown on the cross-sectional SEM micrograph in Figure 3b (secondary electron (SE) mode). Figure 3c depicts the Pt transducer on top of the diamond film through backscattered-electron (BSE) imaging. The BSE image clearly shows the three-layered structure of the sample composed of a Pt layer, a diamond film, and a Si substrate. Diamond growth was observed to occur following the formation of characteristic columnar structures, thus revealing the anisotropic microstructure of the diamond deposit in the transverse and radial directions. In addition, the diamond grain size was observed to increase with the film thickness. A maximum growth rate of 31 μm/h on Si was

achieved through this process, which is much higher than that of conventional CVD techniques. This aspect is of significant importance because a low growth rate in diamond CVD techniques is one of the critical limiting factors for diamond film applications.

It was demonstrated in previous studies that diamond films grown through laser-assisted combustion exhibit high diamond phase purity with the presence of graphitic carbon in the microstructure. The laser resonant excitation of ethylene molecules helps reduce contamination of the diamond film by impurities existing in the harsh open-air growth environment by increasing the concentration of hydrocarbon radicals and atomic hydrogen in the flame environment.[22,23] This promotes the incorporation of sp^3 carbons and etching of sp^2 carbons from the growing surface. The effect of laser excitation on the flame is also remarkable, resulting in a smaller flame size and increased flame velocity.

The impurities existing in the films are incorporated during the growth process and are located at the grain boundaries, which are areas of high surface energy that concentrate the nondiamond elements. The growth of numerous, randomly oriented diamond crystals in the early stage of the deposition process leads to a high concentration of grain boundaries close to the film/substrate interface. Meanwhile, columnar growth dominates in the upper parts of the film, ending up on fewer and relatively larger diamond crystals with fewer grain boundaries. Therefore, it has been established that the columnar microstructure of CVD diamond films leads to increasing diamond phase purity with increasing diamond film thickness.[22]

3.2. Measurements of the Diamond Film Thermal Conductivity and Pt/Dia and Dia/Si Interface Thermal Resistances. The measured amplitude and phase of thermal IR responses obtained from diamond films are plotted as a function of the frequency for various diamond film thicknesses in parts a and b of Figure 4, respectively. The transverse thermal conductivity of the diamond films (k_{Dia}), as well as the TBR at the Pt/Dia interface ($R^i_{Pt/Dia}$) and the TBR at the Dia/Si interface ($R^i_{Dia/Si}$), was estimated from these plots and from the 2D heat-transfer model in the three-layer system. It was found that, for each sample, k_{Dia} was located in the 450−500 W·m^{-1}·K^{-1} range, which is consistent with the range of thermal
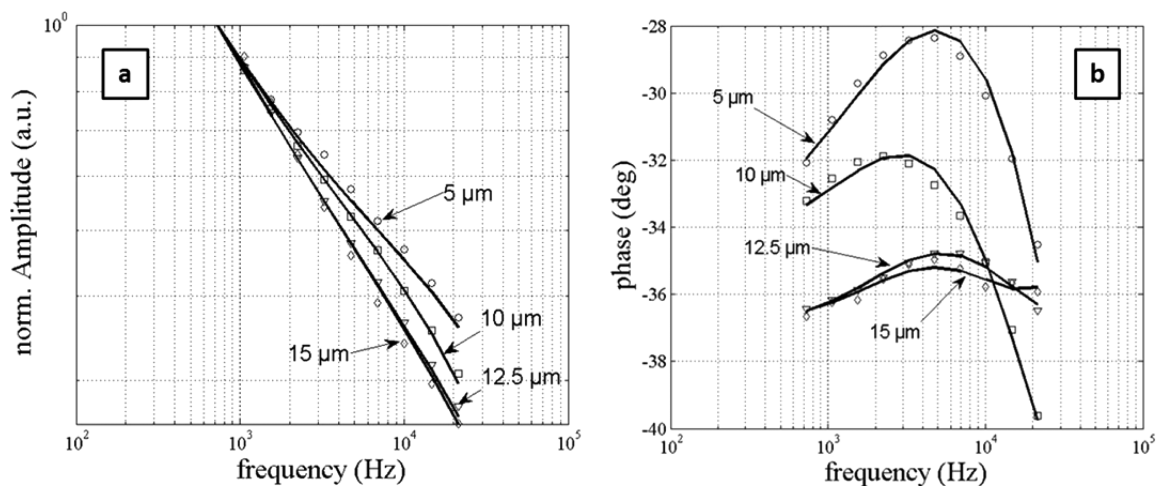

Figure 4. Measured (markers) and simulated (plain lines) (a) amplitude and (b) phase lag of the thermal response of the diamond films with respect to frequency for various film thicknesses.

Table 1. e_{Dia} = Diamond Film Thickness, R_a = Diamond Film Roughness, $R^i_{\text{Pt/Dia}}$ = Measured Thermal Resistance at the Pt/Dia Interface, $R^i_{\text{Dia/Si}}$ = Measured Thermal Resistance at the Dia/Si Interface, $k_{\text{a-Dia}}$ = Thermal Conductivity of the Affected Diamond Layer

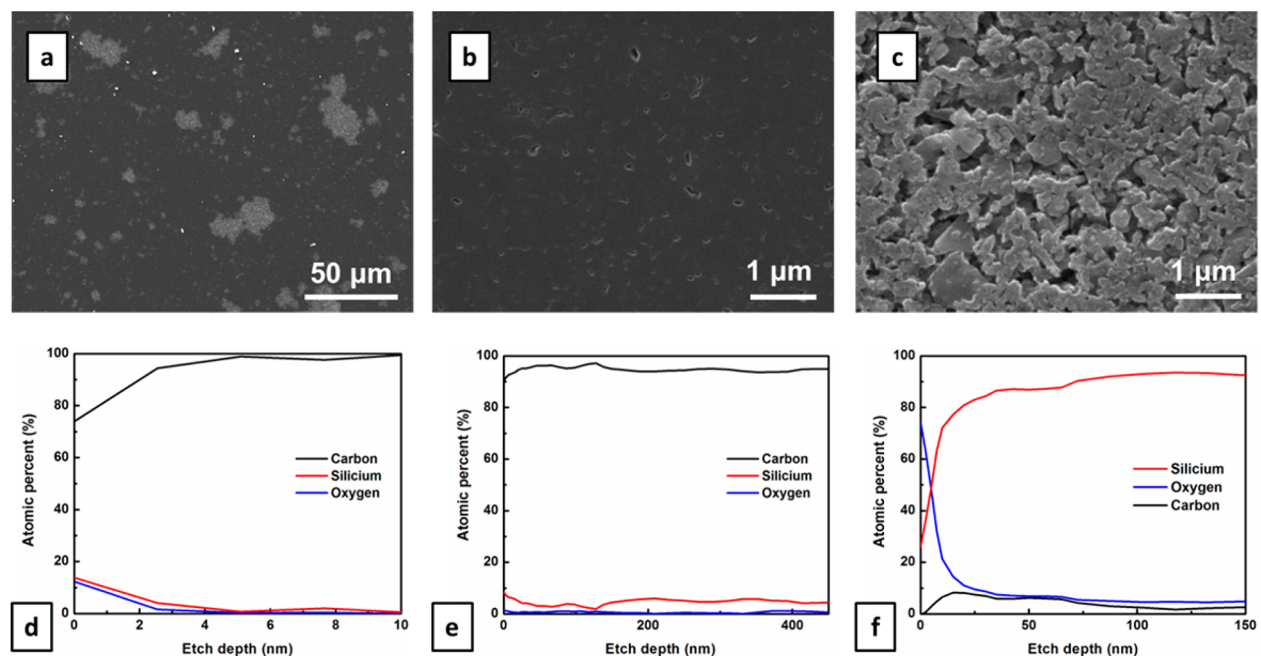| experimental results	e_{Dia} (μm)	5	10	12.5	15
	R_a (nm)	210	380	420	450
	$R^i_{\text{Pt/Dia}}$ ($\times 10^{-7}$ K·m^2·W^{-1})	0.51 ± 0.102	0.91 ± 0.136	0.97 ± 0.145	1.10 ± 0.165
	$R^i_{\text{Dia/Si}}$ ($\times 10^{-7}$ K·m^2·W^{-1})	3.69 ± 0.738	3.09 ± 0.463	1.72 ± 0.258	1.71 ± 0.256
theoretical estimations	$k_{\text{a-Dia}}$ (W·m^{-1}·K^{-1})	1.023 ± 0.204	1.286 ± 0.192	3.117 ± 0.467	3.150 ± 0.472

Figure 5. SEM micrographs of the back face of a diamond film delaminated from a Si substrate: (a) wide-range picture; (b) Si-poor area; (c) Si-rich area. AES in-depth elemental analyses: (d) Si-poor area; (e) Si-rich area; (f) delaminated Si substrate.

conductivity estimations provided in previous studies.[7−10] In addition, this result demonstrates that diamond films grown through the laser-assisted combustion synthesis process are remarkable heat conductors, despite the open-air fabrication conditions propitious to nondiamond content incorporation into the film microstructure. The thermal conductivities obtained were comparable, in terms of heat conduction performance, to those reported for diamond films grown through hot-filament- or microwave-assisted CVD. This is ascribed to the beneficial effect of the multienergy processing conditions in which input from the laser coupled with input from the combustion flame leads to laser-induced resonant excitation of ethylene molecules and an increase in the concentration of active species in the flame environment.

Experimental measurements of yjr diamond film thickness (e_{Dia}) and diamond film roughness (R_a) and experimental estimations of $R^i_{\text{Pt/Dia}}$ and $R^i_{\text{Dia/Si}}$ for the four samples are reported in Table 1. On the basis of the standard deviation for the identified parameters (eq 16 in the SI), uncertainties of 20% on the thermal parameters of the 5-μm-thick diamond film and of 15% on the thermal parameters of the 10-, 12.5-, and 15-μm-thick diamond films are assumed. $R^i_{\text{Pt/Dia}}$ ranged from 0.51 × 10^{-7} to 1.10 × 10^{-7} K·m^2·W^{-1} and slightly increased with the diamond film thickness. This is ascribed to the increase in the surface roughness as the film got thicker, thus leading to an increase in the thermal resistance at the Pt/Dia interface. $R^i_{\text{Dia/Si}}$ ranged from 1.7 × 10^{-7} to 3.7 × 10^{-7} K·m^2·W^{-1}, which

constitutes diamond film/substrate TBR values about 10 times higher relative to those typically reported for diamond films grown by other CVD processes, such as hot-filament- and microwave-plasma-assisted CVD. This demonstrates that, unlike the transverse thermal conductivity of the diamond film, which is affected in a very limited way by the open-air environment, the Dia/Si interface strongly suffers from the open-air processing conditions and exhibits a high level of heat flux resistance relative to Dia/Si assemblies grown through classical vacuum-based CVD methods. In addition, these results demonstrate that the Dia/Si interface is about 10 times more thermally resistive relative to the bulk diamond film, enlightening the critical role played by the interface in the heat conduction process through Dia/Si assemblies. Indeed, the thermal resistance of a 10-μm-thick bulk diamond film with a thermal conductivity of 500 W·m^{-1}·K^{-1} is $R_{\text{Dia}} = e_{\text{Dia}}/k_{\text{Dia}} = 2 \times 10^{-8}$ m^2·K·W^{-1}, thus about 10 times lower than the TBR at the Dia/Si interface reported here.

Because of the high temperature of the deposition process used in this study, it is expected that compounds such as silicon carbide (SiC) and silicon dioxide (SiO$_2$) will be found in the form of additional interfacial layers between Dia and Si. The existence of foreign materials at the Dia/Si interface was sought to be detected through AES analysis. However, no thick interphase was detected using this technique. Figure 5a shows a SEM micrograph of the back face of a diamond film grown through laser-assisted combustion synthesis on a Si substrate
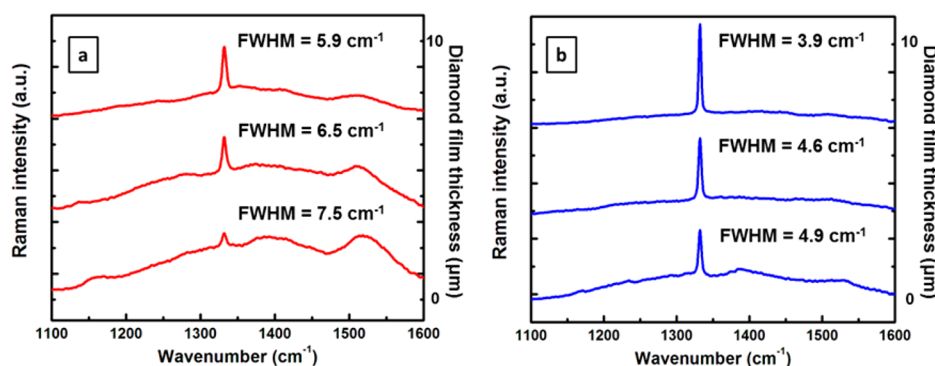
Figure 6. Raman spectra of 10-μm-thick diamond films grown for (a) 20 min and (b) 50 min through laser-assisted combustion synthesis with respect to the film thickness.

and then delaminated. In agreement with the Auger analysis carried out, no thick interphase material was observed. However, it was detected through SEM and AES that Si-rich areas (Figure 5c,e) existed on the back face of the delaminated diamond film among carbon-only zones (Figure 5b,d). In addition, an oxygen-rich layer was detected through AES on top of Si substrates from which diamond films had been delaminated (Figure 5f). From AES analyses, the Si-rich zones of the diamond film and oxygen-rich layer on top of the Si substrate were estimated to be about 300 nm (Figure 5e) and 100 nm (Figure 5f) thick, respectively.

It is known that Si oxidizes upon exposure to oxygen and high temperatures, leading to the creation of SiO_2. Thus, the oxygen-rich layer detected on top of the Si substrate is assumed, in the rest of this paper, to be composed of SiO_2. However, no clear conclusion about the composition of the Si-rich areas located at the Dia/Si interface could be drawn from AES analyses. It has been demonstrated, in previous studies, that cubic silicon carbide (β-SiC) and amorphous silicon carbide (a-SiC) could form at the Dia/Si interface upon diamond growth, but it is not conclusive that SiC existed in the diamond film because the Si-rich areas could have originated from the diffusion of Si atoms into the diamond film with no carbide formation (thus leading to a Si/C solid solution). The interfacial Si/C mixed areas revealed through Auger analysis was assumed to be responsible for the chemical anchorage of the diamond grains to the Si substrate.

The relatively high level of TBR measured at the Dia/Si interface has several sources. One of them is the presence at the Dia/Si interface of foreign materials, such as those detected through AES: SiO_2 originating from Si substrate oxidation and Si/C compounds formed through interatomic diffusion of Si and carbon. The second source contributing to the high level of TBR measured at the Dia/Si interface is the initial roughness of the Si substrate. By laser roughening of the Si substrate to promote diamond nucleation, an additional roughness was introduced at the Dia/Si interface, thus increasing its thermal resistance. Finally, the columnar structure of the films contributed to increased TBR at the Dia/Si interface. Indeed, in the lower layers of the film, the diamond film was made of numerous but randomly oriented and relatively small crystals with a large amount of grain boundaries. Grain boundaries, being surfaces of high energy, constitute preferential locations for the incorporation of impurities. As the deposition process goes on, columnar growth dominates, forming fewer but relatively larger diamond crystals, with the fastest crystallographic growth direction oriented normal to the substrate.

Therefore, imperfections, such as grain boundaries and impurities, exist in large quantity in the layers neighboring the interface, while the upper parts of the film are made of large, single-diamond crystals. Therefore, the phonon mean-free path in the normal direction is longer in the columnar grains of the upper layers of the film relative to the smaller grains in the vicinity of the interface. This helps to explain the strong resistance to the heat flux exhibited by the Dia/Si interface. This also means that the Dia/Si interface considered in this study not only consists of the physical interface separating the film and the substrate but also includes the very first layers (up to 1 μm thick) of the diamond deposit, which are made of a fine-grained structure in which a-SiC, β-SiC, and amorphous carbon (a-C) may be embedded.

It is remarkable that, while the volume thermal resistance of the bulk diamond film was estimated to remain almost constant in the thickness range explored in this study, the TBR between the diamond film and the Si substrate decreased as the diamond film thickness increased. This phenomenon must be due to modifications either in the chemistry or in the microstructure of the lower layers of the diamond films. It is possible that because the thicker samples were exposed to the flame environment for a longer time, thermally activated diffusion and grain growth phenomena may have influenced the structure and composition of the diamond film in the vicinity of the interface with the Si substrate. This assumption is supported by Raman spectroscopic investigations of diamond films with equivalent thicknesses but different times of exposure to the deposition environment (20 and 50 min, respectively). At similar thicknesses, the diamond film exposed to the laser-assisted combustion deposition process for 50 min showed a strongly enhanced sp^3/sp^2 carbon ratio relative to the film grown during 20 min, as shown in Figure 6. Figure 6 also displays the full width at half-maximum (fwhm) of the diamond peak of each spectrum, indicating the diamond phase purity (pure diamond shows a Raman fwhm of 3 cm^{-1}). At equivalent thicknesses, the Raman peak width of the diamond was observed to decrease from 7.5 to 5.9 cm^{-1} for a 20-min grown film and from 4.9 to 3.9 cm^{-1} for a 50-min grown film. This first confirms an increase in the diamond phase purity with the film thickness and an enhancement of the diamond phase purity with exposure to the flame environment. This trend was observed on the whole thickness of the diamond film and is especially remarkable in the lower diamond layers close to the Si substrate. The phase-purity enhancement of the highly resistive lower layers of the film with increased deposition time is assumed to be responsible for the decrease in the thermal
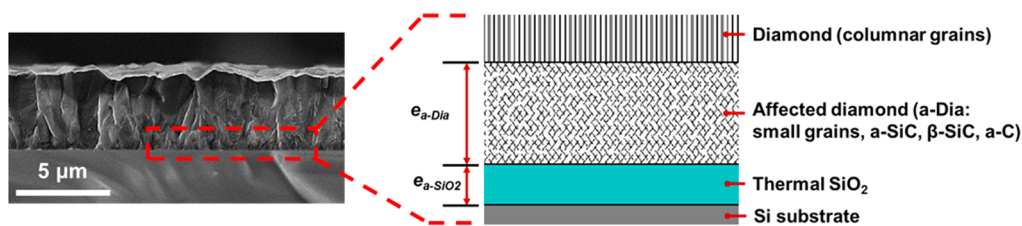
Figure 7. Scheme depicting the model of the Dia/Si interface for TBR estimations through the DMM.

Table 2. Thermophysical Parameters (Θ_D = Debye Temperature, ρ = Density, C_p = Specific Heat, k = Thermal Conductivity, v_l = Longitudinal Phonon Velocity, v_t = Transverse Phonon Velocity) for Pt, CVD Diamond, a-SiC, a-SiO$_2$, and Si at Room Temperature

material	Θ_D (K)	ρ (g·cm^{-3})	C_p (J·kg^{-1}·K^{-1})	k (W·m^{-1}·K^{-1})	$v_l \times 10^6$ (cm·s^{-1})	$v_t \times 10^6$ (cm·s^{-1})
Pt[28,29]	240	24.45	130	71.6	0.4174	0.1750
Dia[30]	2240	3.51	540		1.467	1.281
a-SiC[31]	600	3.05	640	1.2	0.720	0.425
a-SiO$_2$[32,33]	246	2.20	787	1.43	0.663	0.404
Si[34,35]	674	2.33	700	148	0.834	0.590

resistance at the Dia/Si interface with increased film thickness recorded though MPTR experiments.

In conclusion, the interface between the diamond layer and the Si substrate can be viewed as represented in Figure 7. On the basis of the AES results, a thermal SiO$_2$ layer was assumed on top of the Si substrate. Its thickness ($e_{a\text{-SiO}_2}$) was set to $e_{a\text{-SiO}_2}$ = 100 nm. We defined the affected diamond (a-Dia) layer as the layer where a-SiC, β-SiC, amorphous carbon, and small grains of diamond possibly coexisted in the lower parts of the diamond films. On the basis of the AES results, the thickness of this affected diamond layer ($e_{a\text{-Dia}}$) was set to $e_{a\text{-Dia}}$ = 300 nm.

3.3. Theoretical Thermal Resistances at the Pt/Dia and Dia/Si Interfaces. A theoretical estimation of $R^i_{\text{Pt/Dia}}$ and $R^i_{\text{Dia/Si}}$ can be obtained using the diffuse mismatch model (DMM).[28] Because the Debye temperatures of diamond ($\Theta_{D,\text{Dia}}$) and Pt ($\Theta_{D,\text{Pt}}$) are $\Theta_{D,\text{Dia}} \gg \Theta_{D,\text{Pt}}$, the thermal resistance at the Pt/Dia interface was approximated by $R^i_{\text{Pt/Dia}} = 4/(\tau_{\text{Pt/Dia}} C_{p,\text{Pt}}(T) c_{D,\text{Pt}})$, where $C_{p,\text{Pt}}$ is the specific heat of Pt. The phonon transmission coefficient $\tau_{\text{Pt/Dia}}$ was defined as $\tau_{\text{Pt/Dia}} = \sum_{s=l,t} v_{s,\text{Dia}}^{-2} [\sum_{s=l,t} v_{s,\text{Dia}}^{-2} + \sum_{s=l,t} v_{s,\text{Pt}}^{-2}]$ with v_l and v_t denoting the phonon longitudinal and transverse velocities, respectively, and $c_{D,\text{Pt}}$ being the Debye velocity (speed of sound) of Pt, given by $c_{D,\text{Pt}} = (v_l + 2v_t)/3$. Using data reported in Table 2, $R^i_{\text{Pt/Dia}} = 2.125 \times 10^{-8}$ m^2·K·W^{-1}, which is very consistent with the Pt/Dia thermal resistance exhibited by the diamond surface with low roughness. The accuracy of this estimation is, however, affected by the increasing roughness of the diamond surface with increasing film thickness and is no longer valid for thicker diamond films.

The thermal resistance at the Dia/Si interface must be accounted for with the a-Dia layer and the thermal SiO$_2$ (amorphous) layer produced during deposition. It is, therefore, legitimate to estimate the thermal resistance as

$$R^i_{\text{Dia/Si}} = R^i_{\text{Dia/a-SiC}} + e_{a\text{-Dia}}/k_{a\text{-Dia}} + R^i_{\text{a-SiC/a-SiO}_2}$$
$$+ e_{a\text{-SiO}_2}/k_{a\text{-SiO}_2} + R^i_{\text{a-SiO}_2/\text{Si}}$$

where $R^i_{\text{Dia/a-SiC}}$, $R^i_{\text{a-SiC/a-SiO}_2}$, and $R^i_{\text{a-SiO}_2/\text{Si}}$ are the TBR values at the Dia/a-Dia interface, at the a-Dia/a-SiO$_2$ interface, and at the a-SiO$_2$/Si interface, respectively, and are estimated using the DMM described above for the Pt/Dia interface. Knowing that

the Debye temperatures for the four materials are $\Theta_{D,\text{Dia}} > \Theta_{D,\text{Si}} > \Theta_{D,\text{a-SiC}} > \Theta_{D,\text{a-SiO}_2}$, one obtains $R^i_{\text{Dia/a-SiC}} = 3.419 \times 10^{-9}$ K·m^2·W^{-1}, $R^i_{\text{a-SiC/a-SiO}_2} = 9.976 \times 10^{-10}$ K·m^2·W^{-1}, and $R^i_{\text{a-SiO}_2/\text{Si}} = 1.424 \times 10^{-9}$ K·m^2·W^{-1}. Assuming those values do not vary with respect to the diamond film thickness and given the values previously measured of the thicknesses of the a-SiO$_2$ and a-Dia layers and of the thermal resistance at the Dia/Si interface $R^i_{\text{Dia/Si}}$, one finds the theoretical thermal conductivity of the affected diamond layer ($k_{a\text{-Dia}}$) reported in Table 1. It appears clearly that the affected diamond layer has a very low thermal conductivity relative to the bulk diamond film material (k_{Dia} = 450−500 W·m^{-1}·K^{-1}).

4. CONCLUSIONS

MPTR was used to estimate the thermal conductivity and TBR of diamond (Dia) films grown through laser-assisted combustion synthesis on Si substrates. The thermal conductivity of the diamond films was estimated to be located around 500 W·m^{-1}·K^{-1} for all samples investigated, which demonstrates that the diamond films grown through this process are remarkable heat conductors, despite the open-air growth conditions favorable to the incorporation of impurities. MPTR investigations also demonstrated that the TBR at the Dia/Si interface ranged from 1.7×10^{-7} to 3.7×10^{-7} K·m^2·W^{-1} for diamond films with thicknesses ranging from 5 to 15 μm, respectively. MPTR demonstrated that the Dia/Si TBR majorly contributes to the global thermal resistance of the layered assemblies by being about 10 times that of the bulk diamond film. In addition, while the estimated transverse thermal conductivity of the diamond films was found to be in the same range as the values reported for diamond films grown through hot-filament or microwave-plasma-assisted CVD methods, the inceptive layers of the diamond film appeared to suffer from contamination in the early stages of the growth process, thus presenting a strong resistance to the heat flux and contributing to an increased TBR at the Dia/Si interface. Finally, the TBR at the Dia/Si interface was shown to decrease with increasing film thickness. This phenomenon was ascribed to the longer exposure time of thicker samples to the hot flame environment, which triggers diffusion and grain growth phenomena that led to an increase in the diamond phase

2101

dx.doi.org/10.1021/am405188r | ACS Appl. Mater. Interfaces 2014, 6, 2095−2102

purity of the deposit. While the diamond films grown through the laser-assisted combustion synthesis process presented are shown to exhibit promising thermal conductivity, the TBR at the Dia/Si interface appears to be the major limiting factor to their applicability as heat-dissipative materials in electronic packages.

■ ASSOCIATED CONTENT

Ⓢ Supporting Information

Detailed description of the heat-transfer model in the Pt/Dia/Si multilayer sample, of the temperature field, and of the mathematical procedure to retrieve the thermal parameters, a brief description of the fitting procedure based on the Levenberg−Marquardt algorithm, and the expression of the standard deviation for the identified parameters, leading to the uncertainty ranges given in Table 1. This material is available free of charge via the Internet at http://pubs.acs.org.

■ AUTHOR INFORMATION

Corresponding Author
*E-mail: thomas.guillemet@gmail.com. Tel: +33(0)540008810. Fax: +33(0)540008321.

Notes
The authors declare no competing financial interest.

■ ACKNOWLEDGMENTS

■ REFERENCES

(1) Asmussen, J.; Reinhard, D. K. *Diamond Films Handbook*; Marcel Dekker: New York, 2002.

(2) Tong, X. C. *Advanced Materials for Thermal Management of Electronic Packaging*; Springer: New York, 2011.

(3) Goodson, K. E.; Kurabayashi, K.; Pease, R. F. W. *IEEE Trans. Compon., Packag., Manuf., Technol., Part B* **1997**, *20* (1), 104−109.

(4) Looi, H. J.; Pang, L. Y. S.; Wang, Y.; Whitfield, M. D.; Jackman, R. B. *Diamond Relat. Mater.* **1998**, *7*, 565−568.

(5) Jagannadham, K.; Watkins, T. R.; Dinwiddie, R. B. *J. Mater. Sci.* **2002**, *37*, 1363−1376.

(6) Zhang, Z.; Schneider, H.; Tounsi, P. *Mater. Sci. Eng. B* **2012**, *177*, 1358−1361.

(7) Wolter, S. D.; Borca-Tasciuc, D. A.; Chen, G.; Govindaraju, N.; Collazo, R.; Okuzumi, F.; Prater, J. T.; Sitar, Z. *Diamond Relat. Mater.* **2003**, *12*, 61−64.

(8) Takabatake, N.; Kobayashi, T.; Sekine, D.; Izumi, T. *Appl. Surf. Sci.* **2000**, *159−160*, 594−598.

(9) Ho, H. P.; Lo, K. C.; Tjong, S. C.; Lee, S. T. *Diamond Relat. Mater.* **2000**, *9*, 1312−1319.

(10) Jansen, E.; Obermeier, E. *J. Micromech. Microeng.* **1996**, *6*, 118−121.

(11) Plamann, K.; Fournier, D.; Forget, B. C.; Boccara, A. C. *Diamond Relat. Mater.* **1996**, *5*, 699−705.

(12) Leung, K. M.; Cheung, A. C.; Liu, B. C.; Woo, H. K.; Sun, C.; Shi, X. Q.; Lee, S. T. *Diamond Relat. Mater.* **1999**, *8*, 1607−1610.

(13) Majumdar, A. *J. Heat Transfer* **1993**, *115*, 7−16.

(14) Verhoeven, H.; Hartmann, J.; Reichling, M.; Miiller-Sebert, W.; Zachai, R. *Diamond Relat. Mater.* **1996**, *5*, 1012−1016.

(15) Anthony, T. R.; Fleischer, J. L.; Olson, J. R.; Cahill, D. G. *J. Appl. Phys.* **1991**, *69* (12), 8122−8125.

(16) Morelli, D. T.; Beetz, C. P.; Perry, T. A. *J. Appl. Phys.* **1988**, *64*, 3063−3066.

(17) Losego, M. D.; Grady, M. E.; Sottos, N. R.; Cahill, D. G.; Braun, P. V. *Nat. Mater.* **2012**, *11*, 502−506.

(18) Lyeo, H. K.; Cahill, D. G. *Phys. Rev. B* **2006**, *73*, 144301.

(19) Goodson, K. E.; Käding, O. W.; Rösler, M.; Zachai, R. *J. Appl. Phys.* **1995**, *77* (4), 1385−1392.

(20) Verhoeven, H.; Reiss, H.; Füsser, H. J.; Zachai, R. *Appl. Phys. Lett.* **1996**, *69*, 1562−1564.

(21) Stoner, R. J.; Maris, H. J. *Phys. Rev. B* **1993**, *48*, 16373.

(22) Guillemet, T.; Xie, Z. Q.; Zhou, Y. S.; Park, J. B.; Veillère, A.; Xiong, W.; Heintz, J. M.; Silvain, J. F.; Chandra, N.; Lu, Y. F. *ACS Appl. Mater. Interfaces* **2011**, *3*, 4120−4125.

(23) Xie, Z. Q.; He, X. N.; Hu, W.; Guillemet, T.; Park, J. B.; Zhou, Y. S.; Bai, J.; Gao, Y.; Zeng, X. C.; Jiang, L.; Lu, Y. F. *Cryst. Growth Des.* **2010**, *10* (11), 4928−4933.

(24) Battaglia, J. L.; Kusiak, A.; Schick, V.; Cappella, A.; Wiemer, C.; Longo, M.; Varesi, E. *J. Appl. Phys.* **2010**, *107*, 044314.

(25) Kusiak, A.; Martan, J.; Battaglia, J. L.; Daniel, R. *Thermochim. Acta* **2013**, *556*, 1−5.

(26) Veillère, A.; Guillemet, T.; Xie, Z. Q.; Zuhlke, C. A.; Alexander, D. R.; Silvain, J. F.; Heintz, J. M.; Chandra, N.; Lu, Y. F. *ACS Appl. Mater. Interfaces* **2011**, *3*, 1134−1139.

(27) Kelley, C. T. *Iterative methods for optimization*; Society for Industrial and Applied Mathematics: Philadelphia, PA, 1999.

(28) Swartz, E. T.; Pohl, R. O. *Rev. Mod. Phys.* **1989**, *61*, 605−668.

(29) Caffrey, A. P.; Hopkins, P. E.; Klopf, J. M.; Norris, P. M. *Microscale Thermophys. Eng.* **2005**, *9*, 365−377.

(30) Graebner, J. E.; Reiss, M. E.; Seibles, L.; Hartnett, T. M.; Miller, R. P.; Robinson, C. J. *Phys. Rev. B* **1994**, *50*, 3702−3713.

(31) Jeong, T.; Zhu, J. G.; Mao, S.; Pan, T.; Tang, Y. J. *Int. J. Thermophys.* **2012**, *33*, 1000−1012.

(32) Yamane, T.; Nagai, N.; Katayama, S.-I.; Todoki, M. *J. Appl. Phys.* **2002**, *91*, 9772−9776.

(33) Reifenberg, J. P.; Kencke, D. L.; Goodson, K. E. *IEEE Electron Device Lett.* **2008**, *29*, 1112−1114.

(34) Glassbrener, C. J.; Slack, G. A. *Phys. Rev.* **1964**, *134*, A1058−A1069.

(35) Abeles, B.; Beers, D. S.; Cody, G. D.; Dismukes, J. P. *Phys. Rev.* **1962**, *125*, 44−46.